General Disclaimer

One or more of the Following Statements may affect this Document

- This document has been reproduced from the best copy furnished by the organizational source. It is being released in the interest of making available as much information as possible.

- This document may contain data, which exceeds the sheet parameters. It was furnished in this condition by the organizational source and is the best copy available.

- This document may contain tone-on-tone or color graphs, charts and/or pictures, which have been reproduced in black and white.

- This document is paginated as submitted by the original source.

- Portions of this document are not fully legible due to the historical nature of some of the material. However, it is the best reproduction available from the original submission.

5101-176
Low-Cost
Solar Array Project

DOE/JPL-1012-56
Distribution Category UC-63b

Measurement of Surface Recombination Velocity for Silicon Solar Cells Using a Scanning Electron Microscope with Pulsed Beam

Taher Daud
Li-Jen Cheng

November 1, 1981

Prepared for
U.S. Department of Energy
Through an Agreement with
National Aeronautics and Space Administration
by
Jet Propulsion Laboratory
California Institute of Technology
Pasadena, California

(JPL PUBLICATION 81-64)

5101-176
Low-Cost
Solar Array Project

DOE/JPL-1012-56
Distribution Category UC-63b

Measurement of Surface Recombination Velocity for Silicon Solar Cells Using a Scanning Electron Microscope with Pulsed Beam

Taher Daud
Li-Jen Cheng

November 1, 1981

Prepared for
U.S. Department of Energy
Through an Agreement with
National Aeronautics and Space Administration
by
Jet Propulsion Laboratory
California Institute of Technology
Pasadena, California

(JPL PUBLICATION 81-64)

Prepared by the Jet Propulsion Laboratory, California Institute of Technology, for the Department of Energy through an agreement with the National Aeronautics and Space Administration.

The JPL Flat-Plate Solar Array Project is sponsored by the Department of Energy (DOE) and forms part of the Photovoltaic Energy Systems Program to initiate a major effort toward the development of cost-competitive solar arrays.

ABSTRACT

In the design and fabrication of silicon solar cells approaching theoretically ultimate conversion efficiencies, surface recombination velocity plays a crucial role. A technique using a scanning electron microscope with pulsed electron beam has been developed for the measurement of this important parameter of silicon surfaces. It is shown that the surface recombination velocity, s, increases by an order of magnitude when an etched surface degrades, probably as a result of environmental reaction. A textured front-surface-field cell with a high-low junction near the surface shows the effect of minority carrier reflection and an apparent reduction of s, whereas a tandem-junction cell with n^+-p junction near the surface shows an increasing s value.

Electric fields at junction interfaces in front-surface-field and tandem-junction cells acting as minority carrier reflectors or sinks tend to alter the value of effective surface recombination velocity for different beam-penetration depths. A range of values of s from about 10^3 to 10^7 cm/sec has been found for different surfaces.

ACKNOWLEDGMENT

The authors gratefully acknowledge beneficial in-depth discussions with O. von Roos. We also wish to thank K. M. Koliwad for encouragement and help. Technical help in sample preparation and measurement by T. MacConnell, G. Crotty, and J. D. Collier is also appreciated.

This work was done by the Jet Propulsion Laboratory through NASA Task RD-152, Amendment 66, and was sponsored by the U.S. Department of Energy under Interagency Agreement DE-AI01-76ET20356 with NASA.

NOMENCLATURE

A, B, a, b	Constants
D	Diffusion constant
E_b	Electron beam energy
e_i	Ionization energy
f	Function of S and ψ
G	Generation rate of electron-hole pairs
I_b	Electron beam current
I_N	Normalized short-circuit current
I_{N1}, I_{N2}	Values of I_N for different beam energies
I_{sc}	Short circuit or electron beam induced current (EBIC)
k	Back scattering coefficient
L	Minority carrier diffusion length
q	Electronic charge
S	Normalized surface recombination velocity
s	Surface recombination velocity
Z	Normalized junction depth from top surface
z_j	Junction depth from top surface
η	Mean energy loss of back scattered electron
ξ	Depth of beam penetration
τ	Minority carrier lifetime
ψ	Normalized depth of beam penetration

CONTENTS

I. INTRODUCTION 1

II. THEORY 3

III. EXPERIMENT 9

IV. CALCULATIONS AND RESULTS 15

V. DISCUSSION 23

VI. CONCLUSION 25

REFERENCES 27

Figures

1. Parallel Junction Geometry for Scanning Electron Microscope Measurement 4

2. Function f vs Normalized Penetration Depth 7

3. ISI-60A Scanning Electron Microscope 9

4. Column Interior: the Specimen Stage 10

5. Schematic of Measurement Setup 11

6. Configuration of Sample DCO-3 11

7. Front-Surface-Field Cell Configuration 12

8. Tandem-Junction Cell Configuration 13

9. Tandem-Junction Cell 13

10. Short-Circuit Current vs Beam Current for Sample DCO-3 (Case I) 16

11. Short-Circuit Current vs ξ for Sample DCO-3 (Case II) . . . 17

12. Short-Circuit Current vs ξ for Front-Surface-Field Solar Cell 21

13. Short-Circuit Current vs ξ for Tandem-Junction Solar Cell 22

Tables

1. Sample DCO-3 (Case I) 18

2. Sample DCO-3 (Case II) 18

3. Front-Surface-Field Solar Cell with Textured Surface 19

4. Tandem-Junction Solar Cell with Textured Surface 20

SECTION I

INTRODUCTION

The conversion efficiency of solar cells is influenced by cell design and material properties (Reference 1). To design solar cells approaching the highest theoretical conversion efficiency, all parameters related to material and processing must be made optimal. The material property affecting the collection efficiency of light-generated carriers is the minority carrier lifetime τ, which is governed by the recombination rate within the bulk. In addition, charge carriers are lost as a result of the recombination at the surface (References 1, 2).

Surface properties such as charge accumulation sites or surface states, surface potentials, etc., influence the rate of recombination (Reference 3). By analyzing the statistics of recombination through surface states, a method was presented that yielded an explicit expression for surface recombination in terms of the surface potential and the pertinent parameters of the surface states involved (References 4, 5, 6).

The presence of surface recombination in addition to bulk recombination results in a net flow of carriers toward the surface. This is described by the expression surface recombination velocity (s), which is defined as the ratio of the rate of flow of charge carriers into a unit surface area to the excess carrier density in the bulk just beneath the surface (Reference 7).

With the development of materials technology, silicon is slowly evolving with values of τ approaching milliseconds. Techniques of surface preparation of silicon solar cells for reduction of s are necessary; oxidation, front- and back-surface fields, etc. have been tried with some success. A reliable technique for direct measurement of s is therefore needed.

In general, s is derived indirectly from minority carrier lifetime measurements. Effective lifetime, τ_{eff}, as measured, is smaller than the bulk lifetime τ. This effect is used in determining s. Most commonly, τ_{eff} is deduced from conductance measurements under nonequilibrium conditions. The photoelectromagnetic (PEM) effect and the Haynes-Shockley technique have also been used for finding τ_{eff}. Infrared absorption and surface photovoltage techniques are sometimes used for deduction of s. These techniques, however, are indirect and some of them rely on curve fitting for obtaining s.

A more suitable technique for the direct measurement of s for solar cells uses a scanning electron microscope in the electron-beam-induced-current (EBIC) mode. As presented (Reference 8), this method has practical problems of consistency and accuracy because of the surface scattering of the e-beam and requirement of a constant carrier generation rate at low beam energies ($\approx$5 keV).

The analysis and the technique have been refined using a pulsed electron beam in a scanning electron microscope (SEM). The theory of this measurement

is developed in Section II; the experimental procedure is described in Section III. Four different types of solar cell and related surfaces have been used in the experimental determination of ε. A description of the samples is given. Measurement data, calculations, and results are presented in Section IV. Section V contains a discussion of results. Concluding remarks are presented in Section VI.

SECTION II

THEORY

Theoretical models (References 8, 9, 10) have been presented previously for determination of the minority carrier lifetime, τ. Analyses have shown that for sample thickness larger than the minority carrier diffusion length L, the time decay of EBIC is exponential for times greater than minority carrier lifetime, but is affected by s.

For a parallel junction geometry, for a constant rate of carrier generation by the electron beam at different energies, it has been shown (Reference 8) that

$$s = D \frac{\partial}{\partial \xi} (\ln I_{sc}) \Big|_{\xi \to o} \tag{1}$$

where

D = diffusion constant

ξ = penetration depth of the electron beam given by $A(E_b)^B$ with A and B as constants and E_b as beam energy. (Thus $\xi \to o \equiv E_b \to o$)

I_{sc} = short circuit current or EBIC

Electron-hole pair generation rate in silicon (References 11, 12) is given by

$$G = \frac{E_b (1 - k\eta)}{e_i} \cdot \frac{I_b}{q} \tag{2}$$

where

k = back-scattering coefficient

η = mean energy loss of the back-scattered electron

I_b = beam current

e_i = ionization energy required to generate each electron-hole pair

q = electron charge

The assumption of a constant generation rate G for low beam energies ($\geq$8 keV) is difficult to verify in practice because of the large variation of back-scattering coefficient and the mean energy loss of the back-scattered electrons at these lower beam energies. The value of ionization voltage at low energy also varies; values from 29.8 eV to 3.6 eV have been quoted in the literature (References 11, 13, 14) for beam energies of 5 keV to 12 keV. Another practical problem of measurement at low energies is introduced by

surface-scattering variations, which cause inconsistencies in measurements. The analysis that follows is based on no restriction of beam energies and is therefore more amenable to experimental determination of s. First, an exact analysis is presented. Next, since high-efficiency solar cells are more likely to have large L values, an approximate analysis is developed which enables determination of s without the necessity for measurement of L.

Exact Analysis:

When an electron beam impinges on a silicon surface with a parallel junction on the back side (Figure 1), the induced current collected at the junction is given (Reference 15) by:

$$I_{sc} = qG\left[\frac{\cosh\frac{\xi}{L} + S\sinh\frac{\xi}{L}}{\cosh\frac{z_j}{L} + S\sinh\frac{z_j}{L}}\right]$$

or

$$I_N = \frac{I_{sc}}{qG} = \left[\frac{\cosh\frac{\xi}{L} + S\sinh\frac{\xi}{L}}{\cosh\frac{z_j}{L} + S\sinh\frac{z_j}{L}}\right] \qquad (3)$$

where

L = minority carrier diffusion length

S = normalized surface recombination velocity

$= \frac{s \cdot L}{D}$, where D is the diffusion constant

z_j = distance of collecting junction from the top surface

Setting $\psi = \frac{\xi}{L}$ as normalized penetration depth, and taking the derivative of the logarithm of Equation 3:

$$\frac{\partial}{\partial\psi}(\ln I_{sc}) = \frac{\partial}{\partial\psi}(\ln I_N) = \frac{\sinh\psi + S\cosh\psi}{\cosh\psi + S\sinh\psi} \qquad (4)$$

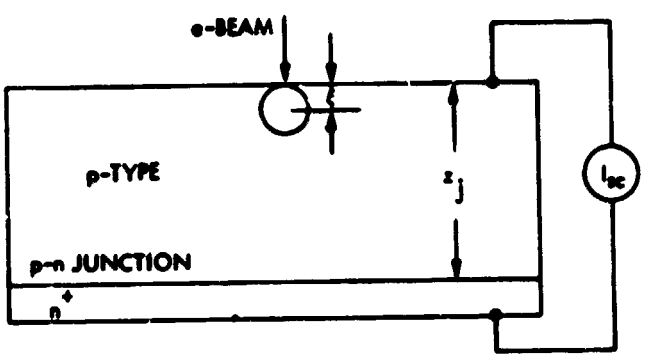

Figure 1. Parallel Junction Geometry for Scanning Electron Microscope Measurement

which can be solved for s to give

$$s = D \frac{\partial}{\partial \psi} (\ln I_{sc}) \left[\frac{\sinh \psi - \cosh \psi \frac{\partial}{\partial \psi} (\ln I_N)}{\sinh \psi \frac{\partial}{\partial \psi} (\ln I_N) - \cosh \psi} \right] \tag{5}$$

Further, substitution of Equation 4 in Equation 5 gives

$$s = D \frac{\partial}{\partial \xi} (\ln I_{sc}) \left[\frac{S (\cosh \psi + S \sinh \psi)}{(\sinh \psi + S \cosh \psi)} \right] \tag{6}$$

Comparison of Equations 6 and 1 shows that removing the restriction of $\xi \to o$ introduces a factor (in brackets) which is a function of S and ψ. Figure 2 shows the variation of $f = \frac{S (\cosh \psi + S \sinh \psi)}{(\sinh \psi + S \cosh \psi)}$ with ψ, with S as a parameter. Another relationship between s and S is given by

$$s = \frac{SD}{L} \tag{7}$$

When Equations 6 and 7 are plotted with measured values of I_{sc} and L, the value of s is obtained as the point of intersection.

Approximate Analysis:

For silicon with diffusion lengths L such that $\psi \ll 1$, Equation 3 can be simplified for two values of ψ (ψ_1 and ψ_2) as

$$I_{N1} = \left[\frac{\cosh \psi_1 + S \sinh \psi_1}{\cosh Z + S \sinh Z} \right] \tag{8}$$

and

$$I_{N2} = \left[\frac{\cosh \psi_2 + S \sinh \psi_2}{\cosh Z + S \sinh Z} \right] \tag{9}$$

where

$Z = \frac{z_j}{L}$ is the normalized junction depth.

This can be further simplified, because of the relationship $\cosh \psi = 1$, and $\sinh \psi = \psi$, as

$$\frac{I_{N1} + I_{N2}}{I_{N1} - I_{N2}} = \frac{2 + S (\psi_1 + \psi_2)}{S (\psi_1 - \psi_2)}$$

giving

$$s = D \frac{(I_{N1} - I_{N2})}{(\xi_1 I_{N2} - \xi_2 I_{N1})} \tag{10}$$

Since this approximation suggests a linear relationship of the form

$$I_N = a + b \cdot \xi$$

where a and b are constants, equation 10 can be written as

$$s = \frac{b}{a} \cdot D \cdot 10^4 \text{ cm/sec} \qquad (11)$$

For Equations 6, 10 and 11 to be valid, the generation rate G at different beam energies has to be held constant. A relationship of $G \propto E_b I_b$ is easier to meet in practice for $E_b \gtrsim 10$ keV.

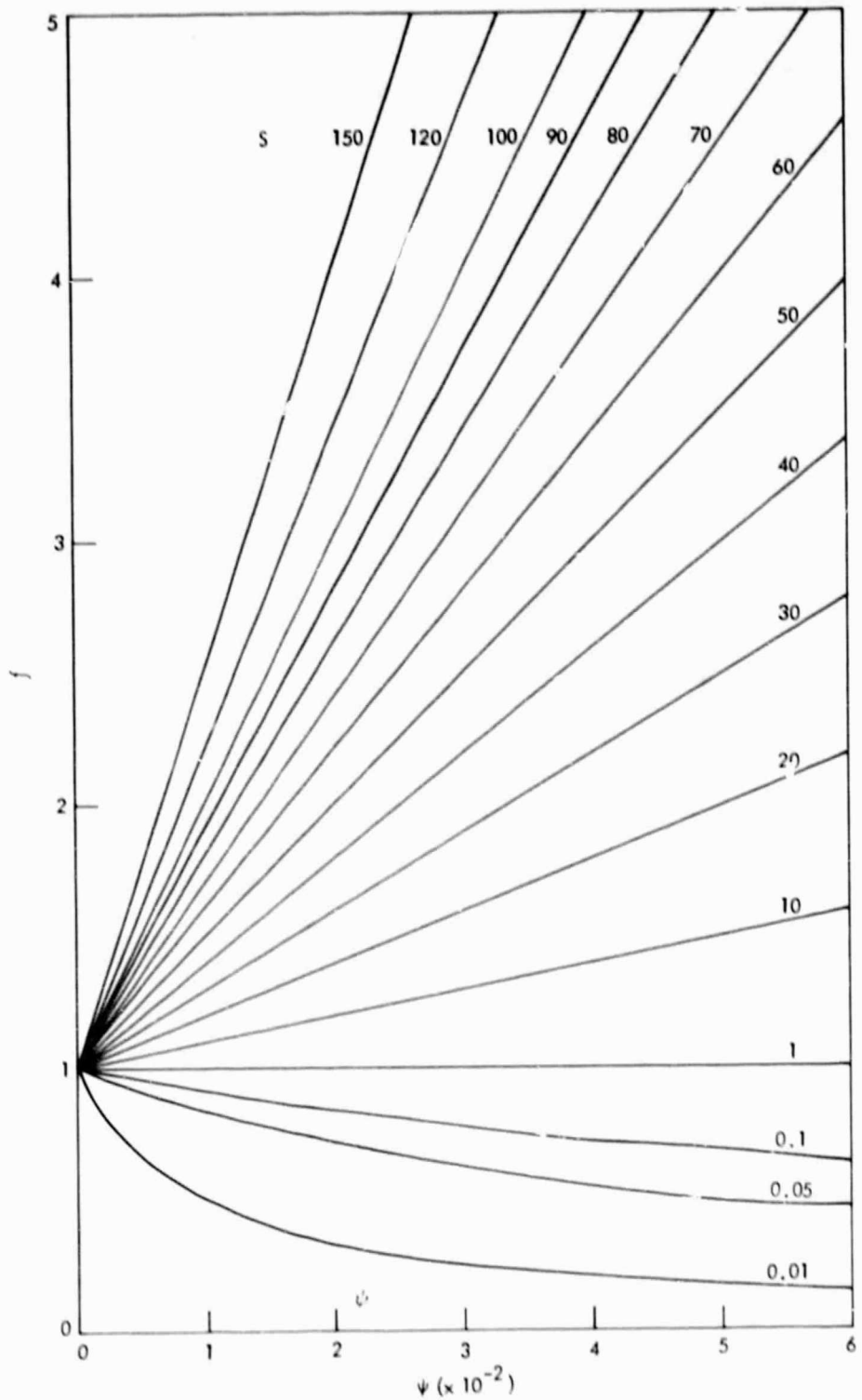

Figure 2. Function f vs Normalized Penetration Depth

SECTION III

EXPERIMENT

The experimental setup consists of an ISI-60A scanning electron microscope (SEM) with beam blanking unit. The beam energy can be varied in steps of 1 keV from 1 to 30 keV. Beam current is measured by a Faraday cup placed near the specimen under test. Beam blanking is operated at 30 Hz. Figure 3 shows an ISI-60A SEM with console and column; Figure 4 shows the specimen stage.

The specimen under test consists of a p-n junction shielded with metal-coated Mylar to absorb reflected electrons from the specimen. The Mylar has an opening of about 1 x 1 mm for beam impingement. The metal on the Mylar sheet is grounded. The signal is brought out by the front and back contacts of the specimen to a PAR 191 current preamplifier. Its output is fed to a lock-in analyzer PAR 5204 and the final reading in millivolts proportional to I_{sc} or EBIC is obtained from a voltmeter connected to the lock-in amplifier. The schematic is shown in Figure 5.

The experimental procedure consists of creating electron-hole pairs in the specimen at different beam energies by a pulsed electron beam. The resulting short-circuit current I_{sc} or EBIC is measured by a digital voltmeter as a proportional voltage output of the lock-in amplifier. For each E_b the data are obtained for a range of beam currents. From these data, relative I_{sc} values for a constant E_b I_b product (hence constant G) are interpolated and utilized for determination of s.

Figure 3. ISI-60A Scanning Electron Microscope

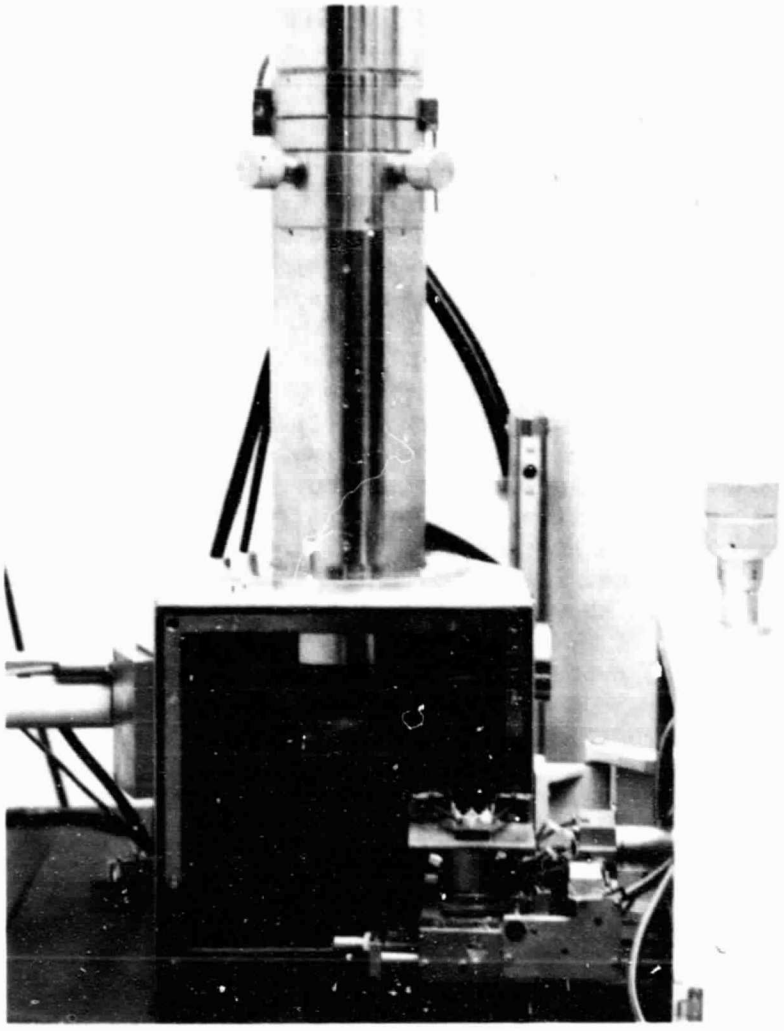

Figure 4. Column Interior: the Specimen Stage

Four different surfaces on three specimens were used in our measurement of surface recombination volocity, as described below:

(1) Sample DCO-3: A 1-Ω-cm boron-doped silicon sample was thermally diffused on the back side with PH_3 to form a junction about 0.5 μm deep. Electrical contacts were made to the surface on the front (p) and back (diffused) side. The specimen configuration is shown in Figure 6. The surface of the specimen was investigated under two conditions. Measurements were made first with the surface freshly etched with $HF:HNO_3$:HAC (Case I), and again after the etched surface was left in the SEM column overnight (Case II).

(2) Sample FSF: A front-surface-field solar cell with ion-implanted front layer of p^+ about 2000 A deep was used for the measurements of s. The cell geometry and measurement configuration is given in Figure 7. It has a texturized front surface and n^+ and p^+ contacts on the back surface.

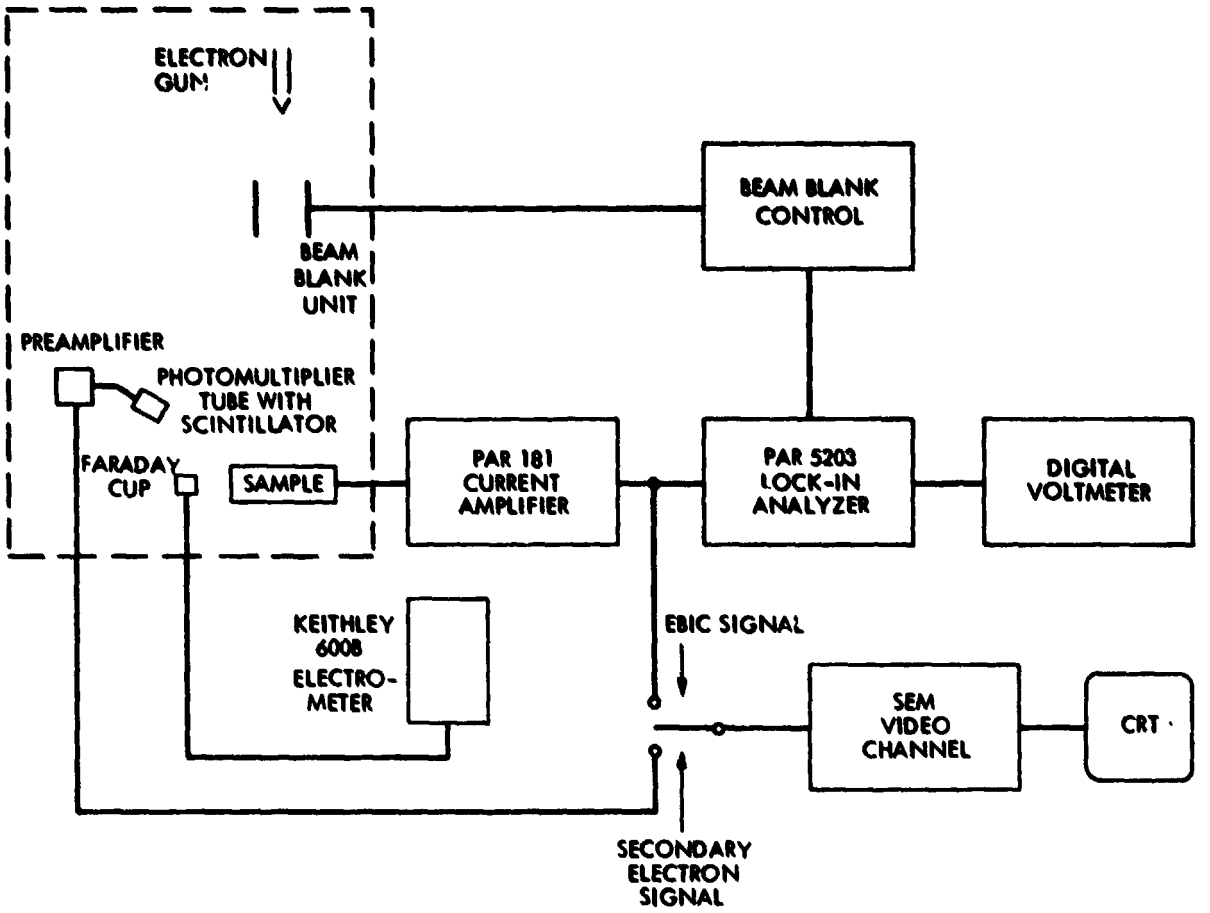

Figure 5. Schematic of Measurement Setup

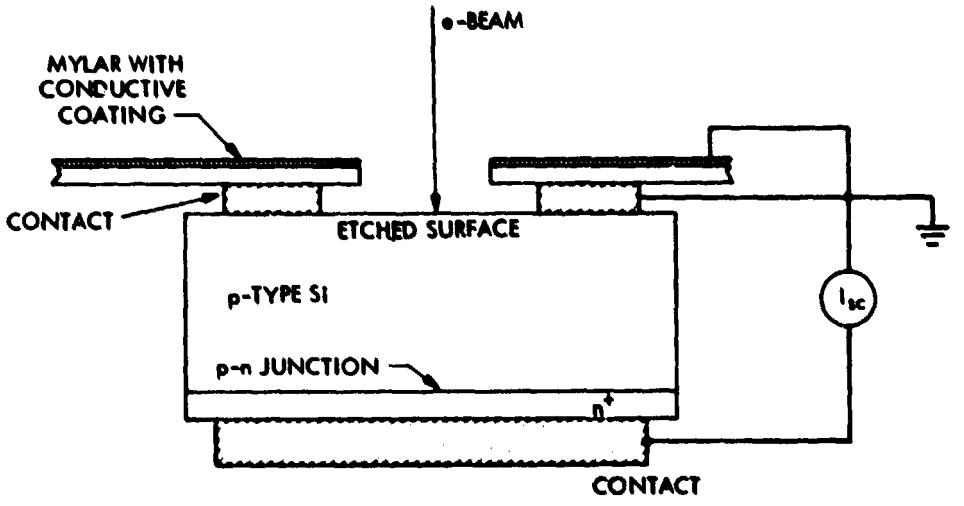

Figure 6. Configuration of Sample DCO-3

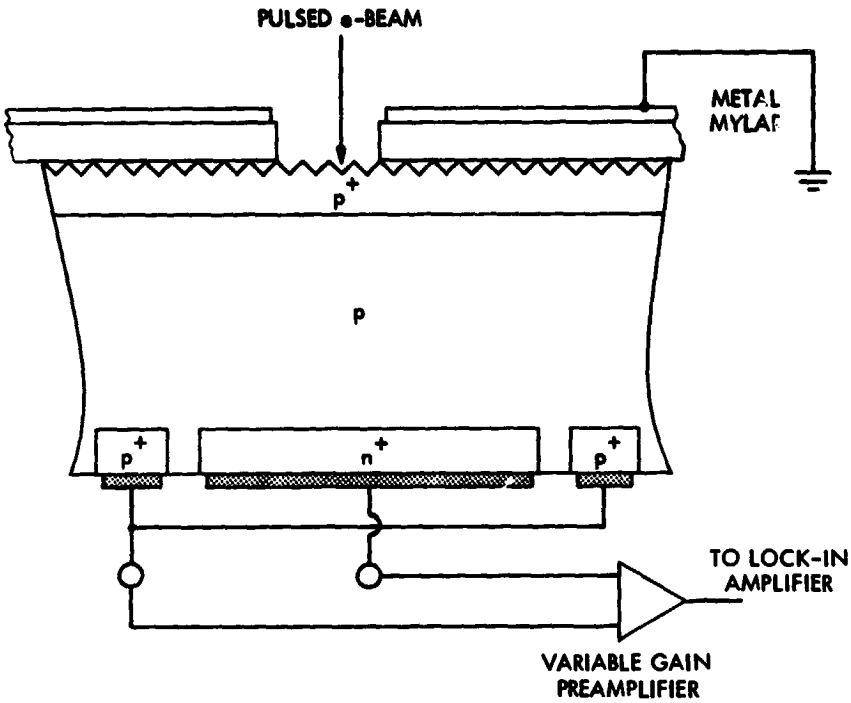

Figure 7. Front-Surface-Field Cell Configuration

(3) Sample TJC: The cell configuration is shown in Figure 8. This is a tandem-junction cell with an n^+ implanted layer on the front with a textured surface. The n^+ and p^+ contacts are on the back side. Figure 9 shows front and back views of the cell.

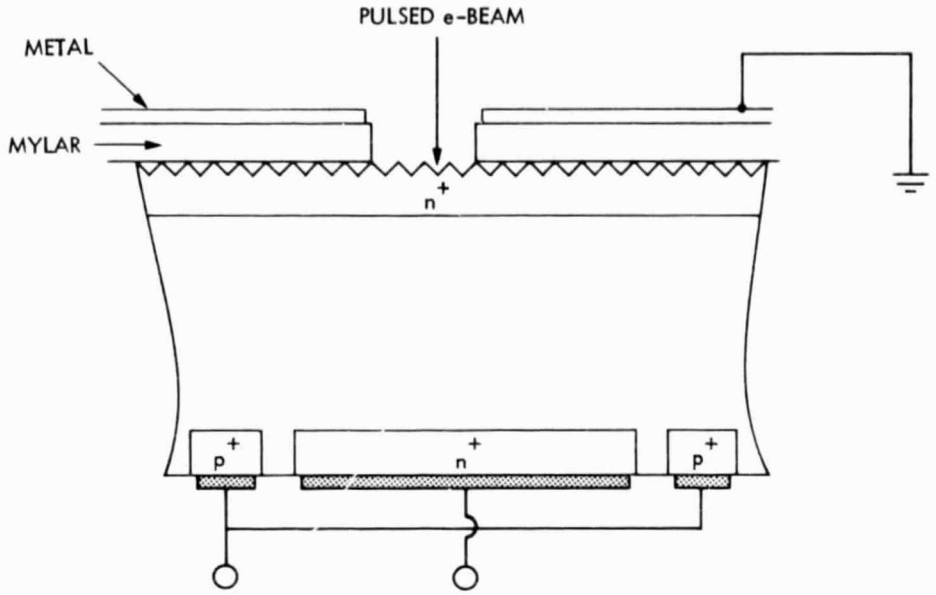

Figure 8. Tandem-Junction Cell Configuration

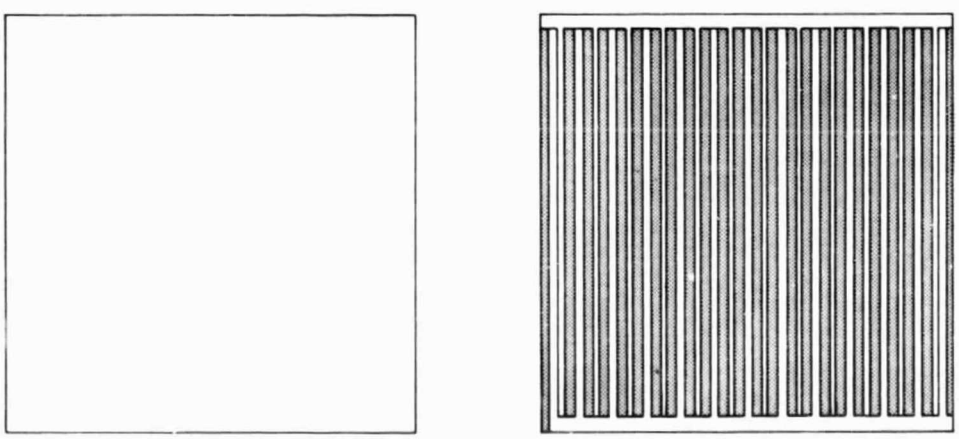

Figure 9. Tandem-Junction Cell

SECTION IV

CALCULATIONS AND RESULTS

Sample DCO-3 (Case I)

The data of voltmeter readings proportional to I_{sc} at various levels of I_b with E_b as a parameter are plotted as Figure 10. For the E_bI_b product of 1.5×10^{-7} electron-volt-ampere (eVA), values of I_{sc} and E_b are given in Table 1. The penetration depth ξ is obtained using the following relationship (Reference 16):

$$\xi = 0.82 \left[E_b \text{ (keV)}\right]^{1.75} \times 10^{-2} \ \mu m$$

Use of Equations 6 and 7:

Also given in the table are the values of $\ln I_{sc}$. The derivatives $\frac{d}{d\xi} \ln I_{sc}$ at mean depths $\xi = 1.1 \ \mu m$ and $2.5 \ \mu m$ are obtained using a least-square fit of the data at 10, 14, 18 and 22, and 22, 26 and 30 keV, respectively.

The value of $L = 120 \ \mu m$ is obtained by using the EBIC technique (Reference 17) on a beveled edge of the sample. This value along with a value of $D = 30 \ cm^2$ per second was used in calculation of s using Equations 6 and 7. By iteration, the points of intersection obtained with values of s are:

$$\xi = 1.1 \ \mu m \qquad s = 4.1 \times 10^4 \text{ cm/sec}$$

$$\xi = 2.5 \ \mu m \qquad s = 3.9 \times 10^4 \text{ cm/sec}$$

Use of Equation 11:

By obtaining a linear fit to the data of Table 1:

$$I_{sc} = 100 \cdot 27 + 13.51\xi$$

giving again

$$s = 4 \cdot 0 \times 10^4 \text{ cm/sec}$$

There is thus a good correlation of results between the exact equations 6 and 7 and the approximation of Equation 11. Further, since the specimens tested here have values of L of 100 m or greater, the condition $\psi \gg 1$ is satisfied. Therefore, Equation 11 is used here for the remaining data.

Sample DCO-3 (Case II)

By a procedure similar to that described above, Table 2 is prepared for the E_bI_b product of 6×10^{-7} eVA giving values of I_b and I_{sc} for E_b from 4 keV to 30 keV. Since for this sample the condition $\psi \gg 1$ is satisfied, and the data give a good linear fit of I_{sc} vs ξ data (Figure 11), s is again

obtained by using Equation 11. Considering readings from 10 to 30 keV, this gives:

$$I_{sc} = 10.76 + 10.96\xi$$

Again taking D = 30 cm^2/sec, s = 3.1 x 10^5 cm/sec, which is an order of magnitude higher than that of a freshly etched sample (Case I above).

FSF Solar Cell Textured with Front Surface Field

Table 3 was obtained from a graph similar to Figure 10. Figure 12 is a plot of I_{sc} vs ξ to show the slow flattening of this curve. This results in a gradual reduction of apparent s from $\approx 10^7$cm/sec at a value of ξ of 0.3 μm to about 8 x 10^3 cm/sec for larger values of ξ. These results are given in the last column of Table 3. This reduction can be explained qualitatively as due to the p^+ region at the silicon surface.

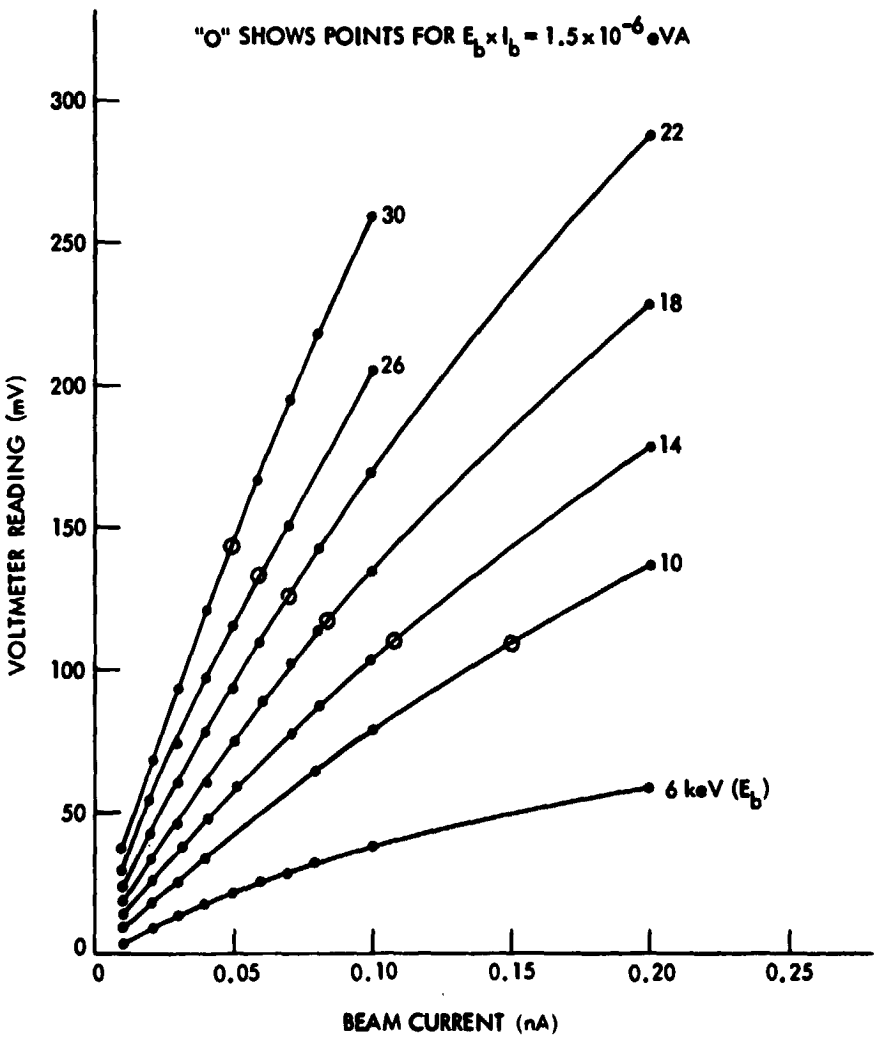

Figure 10. Short-Circuit Current vs Beam Current for Sample DCO-3 (Case I)

TJ Solar Cell

Table 4 was obtained in a manner similar to that of the previous two samples. A plot of I_{sc} vs ξ is given in Figure 13. A comparison of this figure with Figure 11 will show that instead of flattening, the current response increases sharply for deeper beam penetrations. Relevant s values are in the last column of Table 4. In Tables 3 and 4, values of s are obtained by piecewise linear fit of the curves in Figures 11 and 12, respectively, and by use of Equation 11.

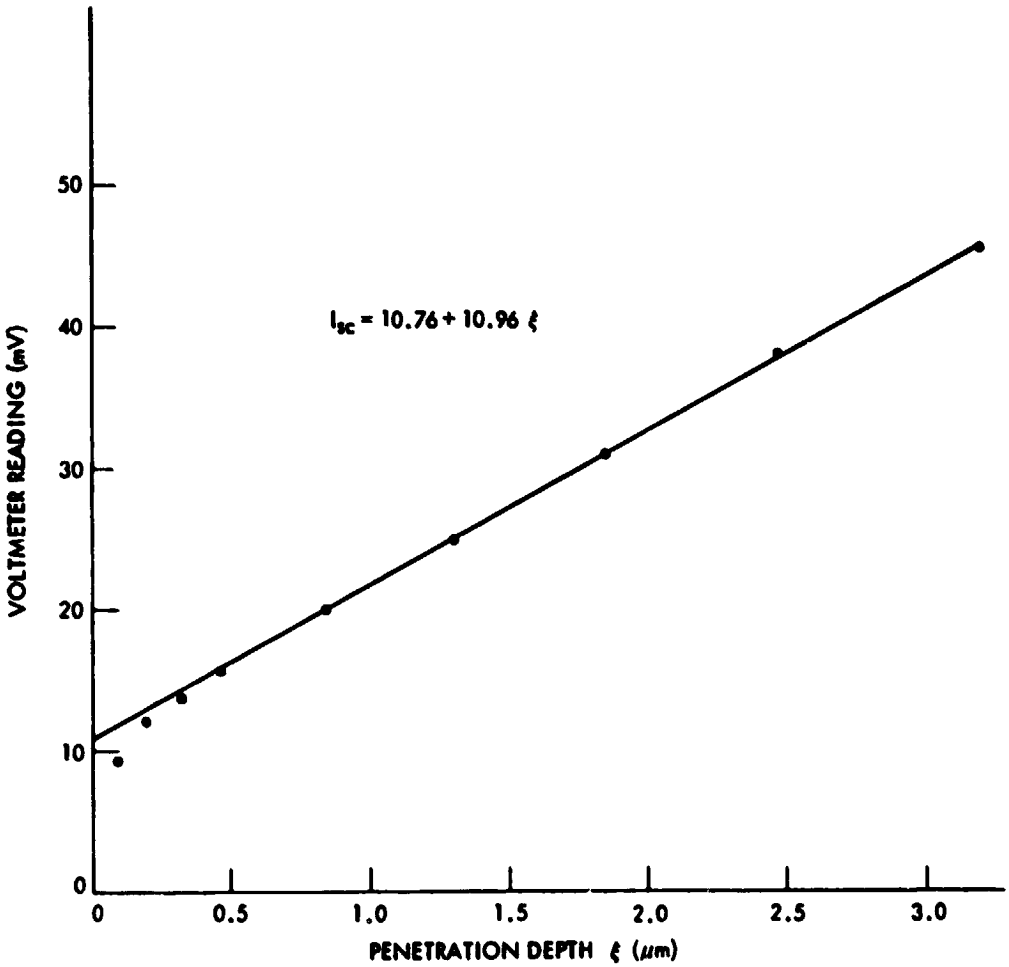

Figure 11. Short-circuit Current versus ξ for Sample DCO-3 (Case II)

Table 1. Sample DCO-3 (Case I)

E_b (keV)	ξ (μm)	I_b (nA)	Voltmeter Reading (mV)	ln I_{sc}	$\frac{d}{d\xi}$ (ln I_{sc}) (per cm)
10	0.46	0.150	108	4.68	
14	0.84	0.107	110	4.70	1.18×10^3 at $\xi = 1.1$ μm
18	1.30	0.083	117	4.76	
22	1.85	0.068	127	4.84	
26	2.47	0.058	132	4.88	9.8×10^2 at $\xi = 2.5$ μm
30	3.18	0.050	144	4.97	

Table 2. Sample DCO-3 (Case II)

E_b (keV)	ξ (μm)	I_b (nA)	Voltmeter Reading (mV)
4	0.09	0.150	9.30
6	0.19	0.100	12.00
8	0.31	0.075	13.75
10	0.46	0.060	15.75
14	0.84	0.043	20.00
18	1.30	0.033	25.00
22	1.85	0.027	31.00
26	2.47	0.023	38.00
30	3.18	0.200	45.50

Table 3. Front-Surface-Field Solar Cell with Textured Surface

E_b (keV)	ξ (μm)	I_b (nA)	Voltmeter Reading (mV)	s (cm/sec)
6	0.19	0.060	48	
8	0.31	0.045	97	$\approx 10^7$
10	0.46	0.036	130	
12	0.64	0.030	170	1×10^6
14	0.84	0.026	197	
16	1.06	0.023	220	1×10^5
18	1.30	0.020	222	
20	1.56	0.018	232	
22	1.85	0.016	250	
24	2.15	0.015	251	3.6×10^4
26	2.47	0.014	265	
28	2.81	0.013	270	8.4×10^3
30	3.18	0.012	270	

Table 4. Tandem-Junction Solar Cell with Textured Surface

E_b (keV)	ξ (μm)	I_b (nA)	Voltmeter Reading (mV)	s (cm/sec)
8	0.31	0.188	11	
10	0.46	0.150	20	
12	0.64	0.125	24	6.3×10^5
14	0.84	0.107	28	
16	1.06	0.094	35	3.3×10^6
18	1.30	0.083	44	
20	1.56	0.075	55	
22	1.85	0.068	63	
24	2.15	0.063	77	
26	2.47	0.058	99	
28	2.81	0.054	117	$\approx 10^7$
30	3.18	0.050	134	

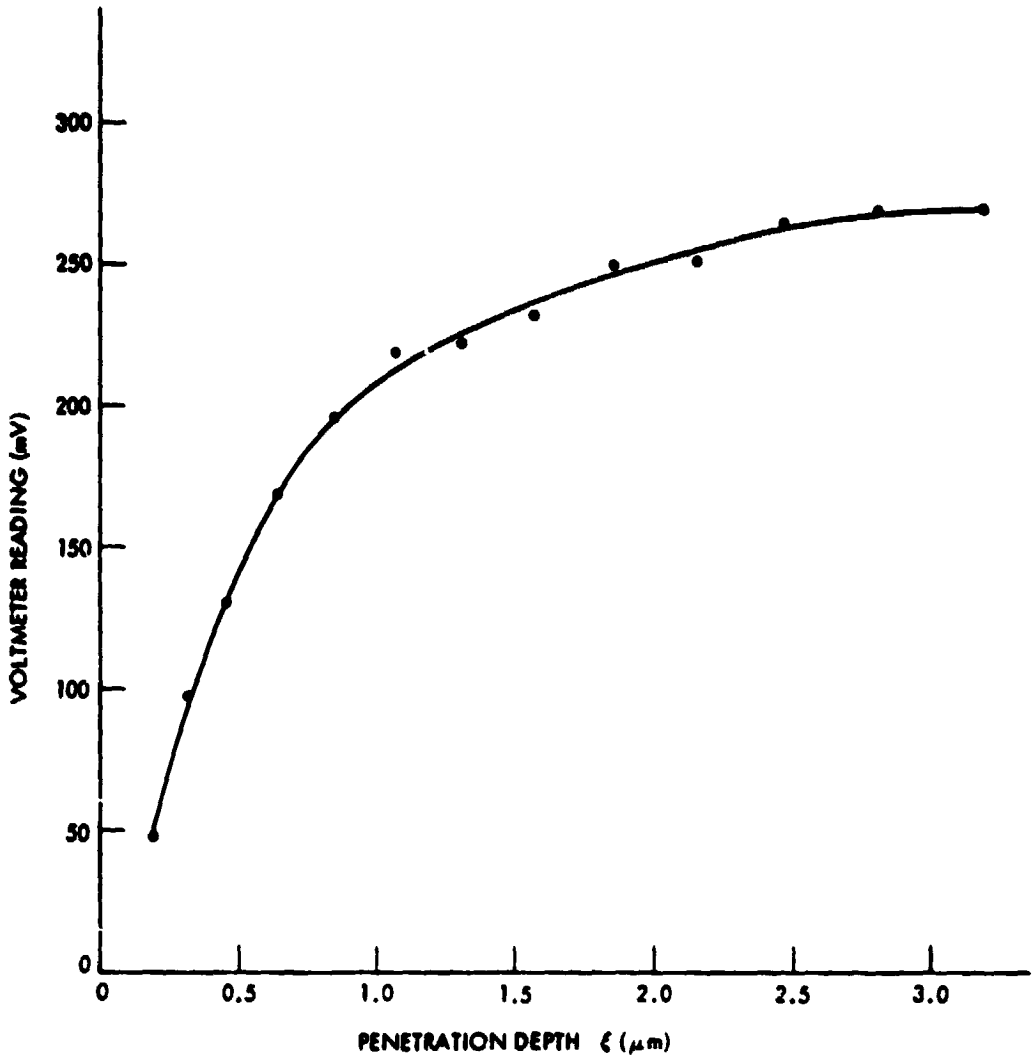

Figure 12. Short-Circuit Current vs ξ for Front-Surface-Field Solar Cell

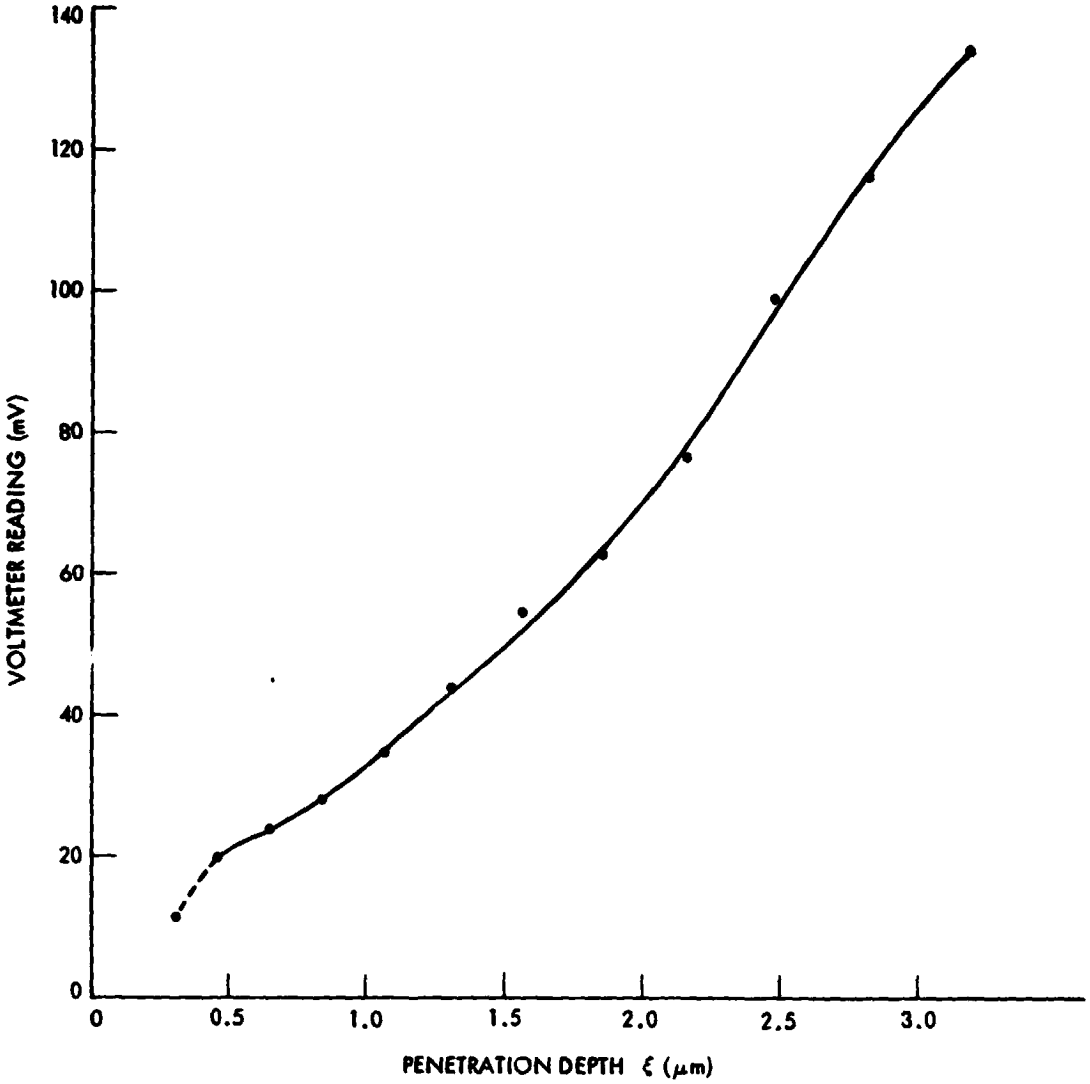

Figure 13. Short-Circuit Current vs ξ for Tandem-Junction Solar Cell

SECTION V

DISCUSSION

There is some discrepancy in the literature regarding the ionization energy required for electron-hole pair creation at low energies. For beam voltages of 12 to 30 keV, values of $e_i = 3.6$ eV have been determined (Reference 14). However, at 5 keV a value as high as 29 eV has been cited. The present results show a good fit of the data from 10 keV to 30 keV with $e_i = 3.6$ eV. The reduction of I_{sc} at $E_b = 4$ keV can be accounted for in these data by considering $e_i = 4.5$ eV.

The readings on the front-surface-field solar cell show a gradual flattening of current response with beam penetration. Part of the generation of electron-hole pairs is very near, or in, the top p^+ layer, susceptible to the high recombination rate of the surface. At greater penetration depth, most of the carrier generation takes place below the top p^+ region. Thus, this p^+ region acts as a reflector for most of the generated minority carriers, and the apparent surface recombination velocity decreases.

For tandem-junction cells with an n^+ layer on top, a reverse effect is observed. Further, at deeper penetration, more generated carriers are able to arrive at the bottom contacts, resulting in a higher electron-beam-induced current. Most of the minority carriers diffusing toward the top contact, however, do not contribute to I_{sc} and recombine at the surface. This results in a higher measured value of s. The values of I_{sc} presumably would saturate at higher ξ values. This larger s value is consistent with the fact that the front junction does not act as a minority carrier reflector until the light induced forward bias becomes significant ($\gtrsim$0.4 volts) (Reference 18).

Electric fields at junction interfaces in FSF and TJ cells acting as minority carrier reflectors and sinks tend to alter the measured value of s for varying depths of carrier generation.

SECTION VI

CONCLUSION

A refined technique for the measurement of surface recombination velocity, s, is presented. Experimental results on solar cells and related geometry demonstrate the usefulness of this technique. A simplified formula has been obtained for silicon in which the minority carrier diffusion length L is large compared with the beam penetration depth. Use of this formula enables determination of s without measuring L. This technique can be used for the study of surface passivation of solar cells. Variation of s values from 8×10^3 to 10^7 cm/sec for different surfaces is obtained. Etched samples have been shown to degrade with time. The effect of minority carrier reflectors and sinks in a front-surface-field solar cell and in a tandem-junction solar cell has been shown.

REFERENCES

1. Hovel, H. J., "Solar Cells," Semiconductors and Semimetals, Vol. 11, Willardson, R. K., and Beer, A. C., Eds., 1975.

2. Bowler, D. L., and Wolf, M., "Interactions of Efficiency and Material Requirements for Terrestrial Solar Cells," Electron Components Conference, April 27-30, 1980.

3. Many, A., et al, "Semiconductor Surfaces," North Holland, 1965.

4. Brattain, W. H., and Bardeen, J., Bell System Tech. J., Vol. 32, p. 1, 1953.

5. Stevenson, D. T., and Keyes, R. J., Physics, Vol. 20, p. 1041, 1954.

6. Many, A., et al, "Semiconductor Surface Physics," Kingston, R. J., Ed., University of Philadephia Press, p. 85, 1957.

7. Shockley, W., "Electrons and Holes in Semiconductors," D. Van Nostrand Co., p. 321, 1963.

8. Watanabe, M., et al, "Determination of Minority Carrier Lifetime and Surface Recombination Velocity with High Spacial Resolution," IEEE Tr., ED-24, p. 1172, 1977.

9. Jakubowicz, A., "Theory of Lifetime Measurements in Thin Semiconductor Layers with the Scanning Electron Microscope; Transient Analysis," Solid-State Electron, Vol. 23, p. 635, 1980.

10. Von Roos, O., "Extension of a Theoroem used in the Investigation of p-n Junctions with the Scanning Electron Microscope to Arbitrary Geometries and Arbitrarily Inhomogenous Material," Applied Physics Letters, Vol. 35, p. 408, 1979.

11. Bresse, J. F., "Electron Beam Induced Current in Silicon Planar p-n Junctions: Physical Model of Carrier Generation. Determination of Some Physical Parameters in Silicon," Scanning Electron Microscopy/1972 (Part I), p. 105, Proceedings of the 5th Annual SEM Symposium, April 1972.

12. Daud, T., "The Effect of Grain Boundaries and Surface Damage on p-n Junction Silicon Solar Cells," Ph.D. Thesis, p. 47-48, University of California, Los Angeles, 1979; Daud, T., and Koliwad, K. M., "Effect of Grain Boundary in Silicon Sheet on Minority Carrier Diffusion Length and Solar Cell Efficiency," JPL Internal Document No. 5101-69, June 1978.

13. Czaja, W., "Response of Si and GaP p-n Junctions to a 5 to 40 keV Electron Beam," J. Appl. Phys., Vol. 37, p. 4236, 1966.

14. Fiebiger, J. R., and Muller, R. S., "Pair-Production Energies in Silicon and Germanium Bombarded with Low-Energy Electrons," J. Appl. Phys., Vol. 43, p. 3202, July 1972.

15. Von Roos, O., "On the Determination of Diffusion Lengths by Means of Angle-Lapped p-n Junctions," Solid St. Electron., Vol. 22, p. 113, 1979.

16. Matsukawa, T., and Shimizu, R., "Investigation of Kilovolt Electron Energy Dissipation in Solids," J. Appl. Phys., Vol. 45, p. 733, 1974.

17. Daud, T., Koliwad, K. M., and Allen, F. G., "Effect of Grain Boundaries in Silicon on Minority-Carrier Diffusion Length and Solar Cell Efficiency," Appl. Phys. Lett., Vol. 33, p. 1009, 1978.

18. Chang, L. J., and Leung, D. C., "Behavior of Interdigitated Back-Contact Solar Cells," Proceedings of the 14th IEEE Photovoltaic Specialist Conference, p. 72, San Diego, California, 1980.